Available online at www.sciencedirect.com
ScienceDirect
Journal of Magnetic Resonance 185 (2007) 164–172
JMR Journal of Magnetic Resonance
www.elsevier.com/locate/jmr

Communication

Radiation-damping effects in a birdcage resonator with hyperpolarised ^{3}He gas NMR at 1.5 T

Kevin Teh [a], Nicola de Zanche [b], Jim M. Wild [a,*]

[a] Unit of Academic Radiology, University of Sheffield, Sheffield, England S10 2JF, UK
[b] Institute for Biomedical Engineering, University and ETH, Zurich, Switzerland

Received 9 August 2006; revised 9 November 2006
Available online 15 December 2006

Abstract

The presence and diagnosis of radiation damping could have major implications in NMR experiments with hyperpolarised gases, where accurate knowledge of the flip angle is imperative. In this work radiation damping was observed and investigated in a low-pass birdcage resonator ($Q = 250$) with samples of hyperpolarised ^{3}He at 1.5 T. With an initially highly polarised ($P = 38\%$) sample of ^{3}He in a spherical cell, the observed FID had a distorted line shape with a spectral line width that was three times that of the same sample in a virtually depolarised state (1 Hz line width for $P < 1\%$). Moreover a linear relation between the sample's magnetisation (M_0) and the line width of the spectrum was observed which is indicative of radiation damping. With highly polarised samples, significant radiation damping was observed and the effect was a lower than expected rate of depletion of M_0 in RF flip angle calibration experiments, which led to significant underestimate of the RF flip angle. To our knowledge this is the first report of radiation damping in a birdcage resonator with samples hyperpolarised or otherwise. Experimental observation of radiation damping could be used as means of measuring coil efficiency as an alternative to the geometrical filling factor (η) the definition of which is open to question for a birdcage resonator. Estimates of the birdcage filling factor from the measured damping time constants ($\eta_{RD} = 0.4\%$) are compared to those derived from electromagnetic energy ratios ($\eta_E = 1.6\%$) and metallic sphere frequency shift methods ($\eta_{fs} = 1.4\%$). These figures are much lower than the simple volume geometrical upper limit of $\eta_v = 3.7\%$ derived from the ratio of cell volume to total coil volume (shield included). The physical explanation for this shortfall is that the bulk of the magnetic energy stored in the birdcage is spatially distributed predominantly between the rungs and the shield, and not in the coil centre where the sample is placed and where the B_1^+ field has its highest spatial homogeneity.

Keywords: RF coil; Helium-3; Hyperpolarised; Radiation damping; Birdcage

1. Introduction

Bloch's equations [1] assume the spin ensemble is free from non-linear spin-coupling effects and the longitudinal and transverse relaxation times can be characterised by constants. In the presence of non-linear spin-coupling effects the classical Bloch equations do not fully describe the transverse relaxation mechanism. Such effects can result from intra-molecular spin-coupling perturbations such as J coupling, from long-range coupling interactions such as the dipolar demagnetising field [2] or from back reaction fields from the induced current in the probe (radiation damping) [3]. All of these effects can introduce non-linear behaviour to the spin magnetisation dynamics and the resulting experimental line shapes can be severely distorted [3–5]. In this work attention is focused on radiation damping, which to date has only really posed problems in high-resolution ^{1}H NMR with small coils at high field strengths (>7 T). However the effect may become more of an issue in in vivo NMR and MRI with the prevalence of higher B_0 field strengths, novel polarisation enhancement methods and improved quality factor (Q) of coils [6].

* Corresponding author. Fax: +44 114 272 4760.
E-mail address: j.m.wild@sheffield.ac.uk (J.M. Wild).

1090-7807/$ - see front matter © 2006 Elsevier Inc. All rights reserved.
doi:10.1016/j.jmr.2006.11.009

Radiation damping is an effect caused by the interaction between the sample magnetisation and the tuned RF resonator [3]. It can be classically described as the action of a 'counter' field produced by the current induced in the coil, which exerts a torque opposite to that of the transmit field (B_1^+) to 'push back' the sample magnetisation towards the longitudinal direction. In a quantum description, radiation damping has been described as a spontaneous emission or maser effect [7]. In NMR experiments with short T_2^* or MR imaging experiments where gradients cause rapid dispersion, radiation damping is less likely as the interaction between the transverse magnetisation and the coil is rapidly quenched. In the original analysis of Bloembergen and Pound [3], the temporal envelope of the radiation-damped FID was derived as $\mathrm{sech}(t/\tau_{\mathrm{rd}})$ where the damping time constant is

$$\tau_{\mathrm{rd}} = (2\pi\gamma\eta M_0 Q)^{-1} \tag{1}$$

where M_0 is the longitudinal magnetisation, Q is the quality factor, and η is the filling factor. Gueron et al. [8] gave the damping time constant in SI units as $\tau_{\mathrm{rd}} = (\gamma\eta m_0 Q\mu_0/2)^{-1}$, with m_0 now denoting the longitudinal *magnetisation density*. Should the effects of radiation-damping cause problems in NMR experiments, steps can be taken to desensitise the NMR detection system to radiation damping by active Q damping of the tuned circuit or gradient spoiling of the transverse magnetisation.

Hyperpolarised (HP) gas NMR has the potential for very high M_0 by virtue of the high polarisations that can now be attained ($P > 60\%$) with optical pumping spin exchange techniques. Thus HP gas NMR is potentially very susceptible to radiation-damping and the effects have been described previously in low field HP ^{3}He gas NMR [9], where T_2^* is very long, and also in HP ^{129}Xe gas NMR [10] using adiabatic half passage pulses. Both of these reports are from experiments conducted with small pick-up coils with high Q and good η.

In this work, radiation-damping effects were investigated with HP ^{3}He samples at 1.5 T, using a volume optimised birdcage transmit–receive coil. Birdcage resonators have spatially homogeneous B_1^+ field profile [11], which is important in HP gas MRI with its inherent sensitivity to flip angle due to the non-renewable polarisation. The accurate definition and calculation of η for a birdcage resonator, and its relationship with Q is also an important subject of discussion [12,13] and indeed it has been suggested that sensitivity to radiation damping may be a means of measuring η [13]. This is believed to be the first report of radiation damping in a birdcage resonator with samples either hyperpolarised or thermally polarised.

2. Theory

2.1. Radiation damping

Various vector depictions of the fields describing the radiation-damping effect have been given. Almost all are based on the original classical electromagnetic description by Bloembergen and Pound [3], of a near-field mutual inductance between the transverse magnetisation and the coil with a vector model of the associated magnetic fields [14]. More recently a vector treatment was given that encompasses both the contributions of dipolar demagnetising fields and radiation damping [15]. The theoretical analysis used here is simplified by treating the transverse magnetisation as a single isochromat using the vector treatment of Augustine [16]. This is a valid model for the spin ensemble of the monatomic ^{3}He gas in the absence of long-range dipolar field coupling.

The transmit field which flips the spins from the longitudinal direction to the transverse is given by B_1^+ [17]. After the transmit pulse, and in the presence of a large coherent transverse magnetisation, the current it induces in the coil can create a field, $B_{1\mathrm{R}}(t)$, counter to the transmit B_1^+ (i.e. having opposite phase), which acts to restore the net sample magnetisation back towards the longitudinal direction (reverse back reaction). If $B_{1\mathrm{R}}(t)$ is defined as the time-varying component of this counter RF reaction field near the Larmor frequency (ω_0). Then this reaction field precesses in the transverse plane and is 90° out of phase with the transverse magnetisation vector $(\mathbf{x}\cdot M_x(\delta_\omega,t) + \mathbf{y}\cdot M_y(\delta_\omega,t))$. The magnitude is given by $|B_{1\mathrm{R}}(t)| = (M_x^2(\delta_\omega,t) + M_y^2(\delta_\omega,t))^{1/2}/(\gamma\tau_{\mathrm{rd}}M_0)$ [16], where δ_ω is the offset between ω_0 and the circuit's resonant frequency $\omega = 1/\sqrt{\mathrm{LC}}$.

This effect will thus be prominent when the transverse magnetisation is long-lived (transverse relaxation times are long) allowing a long time for $B_{1\mathrm{R}}(t)$ to act. The FID will have a line-shape that is non-exponential and has been derived by analytical solution of the non-linear Bloch equations as was first demonstrated by Bloom [14]. If the magnetisation vector is considered as a single isochromat in the absence of transverse relaxation (field inhomogeneity broadening) the envelope of the FID is given by $\mathrm{sech}(t/\tau_{\mathrm{rd}})$. If other sources of transverse relaxation are to be included then solution of the non-linear Bloch equations becomes more complicated and may require numerical solution, particularly in the presence of additional field perturbations such as the presence of a dipolar-demagnetising field. For the purpose of this work the ^{3}He transverse magnetisation is treated as a single isochromat and a detailed analysis of the solution to the relaxation was not pursued as the primary objective.

2.2. Hyperpolarised (HP) gas NMR theory

Hyperpolarised (HP) gas (^{3}He and ^{129}Xe) NMR utilises the high M_0 that is produced by optical pumping spin exchange. These polarisations can exceed those of thermal equilibrium NMR of the same nuclei at standard field strengths by a factor of 4–5 orders of magnitude. Conventionally the optical pumping laser emission is circularly polarised so as to create a hyperpolarisation of the nuclear spin ground state, thus creating a magnetisation that can

be manipulated with RF excitation in NMR experiments. However reversal of the direction of the laser $\lambda/4$ circular polariser will create a hyperpolarisation of the excited spin state. Such a state is prone to spontaneous emission in the presence of thermal noise fluctuations at the Larmor frequency in a tuned circuit of high Q. Thus the shape of the radiation damped FID received by a high Q coil from an optical pumping cell is a practical diagnostic means of determining the direction of polarisation produced by the $\lambda/4$ polarising plate in the optical pumping apparatus [18].

Unlike thermally polarised NMR, the hyperpolarised M_0 is non-recoverable and is progressively diminished after application of each B_1^+ RF pulse, ultimately returning to a much smaller thermal equilibrium polarisation. If a series of single pulse acquisitions are performed with constant flip angle α, followed by complete dephasing of the transverse magnetisation with spoiler gradients, then the decay of the transverse signal amplitude with each successive RF pulse (n) is given by

$$M(n) = M_0 \exp(-t/T_1) \cdot \cos(\alpha)^{n-1} \sin\alpha \tag{2}$$

This allows a linear fit to the cosine of the apparent flip angle α

$$\ln[M(n)/M(1)] = (n-1) \cdot \cos(\alpha) - t/T_1 \tag{3}$$

If radiation damping is present the longitudinal magnetisation will be replenished by the back reaction between RF excitations and a non-linear curve will be seen when the expression in Eq. (3) is plotted. The net effect is a smaller observed flip angle α when the relation of Eq. (3) is fit to the data from an RF calibration experiment consisting of a series of spoiled pulse-acquire FIDs. This approach was used to diagnose radiation damping by Wong et al. [9] in low-field experiments with HP ^{3}He using small receiver coils.

2.3. Birdcage filling factor calculations

The coil filling factor (η) is a parameter that has different definitions and several practical means of its measurement are in use. For certain coil designs such as a tightly wound solenoid, simple approximations can be made for η by calculating the ratio of sample volume to the coil volume (η_v), [19]. This is based on the uniform B_1^+ field experienced throughout the coil. Consider a definition for η in an RF coil that produces in general an elliptically polarised field

$$\eta_E = 2\frac{E^+_{\text{Sample}}}{E_{\text{Total}}} \tag{4}$$

where E^+_{Sample} is the time-averaged energy in the B_1^+ field stored in the sample, and E_{Total}, is the total time-averaged energy in the RF magnetic field (B_1). Time averaging is intended over an integral number of periods and will affect primarily the denominator since the instantaneous total magnetic energy in a linearly polarised coil is oscillatory, while in a symmetric quadrature coil it can indeed be constant. This definition is consistent with previous definitions [12] as well as that for the linearly polarised case [3].

In the case of the approximately uniform field produced within a circularly polarised birdcage coil, E^+_{Sample} can be calculated as

$$E^+_{\text{Sample}} = \frac{1}{2}\int_{V_{\text{Sample}}} \frac{|B_1^+|^2}{\mu_0}\,\mathrm{d}V = \frac{1}{2} V_{\text{Sample}} \frac{|B_1^+|^2}{\mu_0} \tag{5}$$

where the temporal averaging has been omitted since $|B_1^+|$ is constant. In a shielded birdcage coil the bulk of the magnetic energy is found between the rungs and the shield where the fields are highest and less so in the coil centre where the sample is placed, where the B_1^+ field has the highest spatial homogeneity. The temporal maximum of magnetic field amplitude in a linear-mode birdcage, or the constant circularly polarised field amplitude of an ideal quadrature birdcage coil may be calculated in the long-cylinder approximation [20] from the sinusoidally distributed currents flowing in the rungs, as

$$B_1 = \frac{\mu_0 I_0 N}{4\pi}\left(\frac{1}{r} - \frac{r}{R^2}\right) \tag{6}$$

The birdcage coil used (see Section 3) has $N = 12$ rungs of length 19 cm, a shield radius $R = 11$ cm, and coil radius $r = 7.5$ cm. In the following calculations a maximal rung current I_0 of 1A was assumed, without restricting the validity of the expressions. This gives $|B_1^+| = 8.6\ \mu\text{T}$ and with a 1 L sample, $E^+_{\text{Sample}} = 29.2$ nJ.

At resonance, peak modal magnetic and electric energies must be equal. The electric energy in a birdcage resonator is stored almost exclusively in the capacitors; the nth capacitor will store an amount

$$E_n = \frac{1}{2}CV^2 = \frac{1}{2}\frac{I_n^2}{\omega^2 C} \tag{7}$$

where $I_n = I_0 \cos(2\pi n/N)$ is the current carried by the capacitor assuming a low-pass birdcage topology. If all currents in the coil's legs are in phase (a reasonable assumption for a moderately damped resonance) the total electric energy is obtained by summation of the energy stored in each capacitor [21]

$$E_{\text{Total}} = \frac{1}{2}\sum_{n=0}^{N-1} \frac{\left(I_0 \cos(\frac{2\pi}{N}n)\right)^2}{\omega^2 C} \tag{8}$$

Eq. (8) can be simplified with the summation,

$$\sum_{n=0}^{N-1}\left(\cos\frac{2\pi}{N}n\right)^2 = \frac{N}{2} \tag{9}$$

giving the total magnetic energy as

$$E_{\text{Total}} = \frac{NI_0^2}{4\omega^2 C} \tag{10}$$

This will give a total energy of 0.98 μJ with the 33 pF rung capacitors used in this coil at f_0 of 48.5 MHz. Dividing the two energies from Eq. (4), bearing in mind that for the quadrature coil no time averaging is required

since magnetic energy is constant, gives $\eta_E = 6.0\%$ for a 1-L sample. Note this is much less than the simplistic geometrical ratio ($\eta_v = 13.8\%$) as derived from the ratio of the 1-L sample volume to the total coil volume. The theoretical calculations shown above are based on the assumption of a long coil, uniform field within the sample and neglecting any stray capacitance that may be present between the coil's conductors. Stray capacitances may be incorporated into the energy calculations, as suggested by the anonymous reviewer, by first re-tuning the birdcage to a higher frequency and then fitting to estimate the additional capacitance values that account for deviations between measured resonant frequencies and those predicted by the applied change in capacitance (i.e. nominal capacitor values).

Alternative empirical methods to determine the experimental magnetic filing factor have been shown by Doty et al. [12]. This "frequency shift" methodology entails placing a small metal sphere of volume V_M into the homogeneous circular polarisation sample region occupied by the sample, V_S, the magnetic filing factor is then given by

$$\eta_{fs} = \frac{4 f_\delta V_S}{3 f_0 V_M} \tag{11}$$

whereby f_δ is the shift in resonant frequency, f_0, when the metal sphere is introduced. Eq. (11) will only be accurate when placed in a uniform transverse magnetic field with low electric fields and negligible axial fields.

3. Materials and methods

NMR measurements were conducted on a 1.5 T whole body MRI system (Eclipse-Philips Medical Systems, Cleveland, OH). The system was fitted with a T/R circuit for ^{3}He at 48.5 MHz. The ^{3}He gas (Spectra Gases, UK) was polarised on site by optical pumping at 795 nm with rubidium spin exchange apparatus (General Electric Medical Systems, Princeton, NJ). This apparatus is capable of polarising approximately 1.8 bar L of ^{3}He to a polarisation of around 40% in a spin-up period of around 24 h. Experiments were performed using three separate gas phantoms: (i) a 3 L polythene bottle which was used as a flood phantom to measure the spatial B_1^+ profile of the coil (T_1 of ^{3}He in bottle ≈5 min), (ii) 1 L Tedlar plastic bags (T_1 of ^{3}He in bag ≈20 min) and (iii) a 270 ml spherical glass cell (Pyrex, T_1 of ^{3}He in cell >1 h). The ^{3}He polarisation was measured inside the optical pumping cell as 27% for the bag experiments and 38% for the cell experiments. The magnetisation density of the samples was calculated from $m_0 = \mu PN/2$, where μ is the nuclear magnetic moment of ^{3}He and N is the number of ^{3}He atoms per unit volume. In the bottle phantom experiments, 100 ml ^{3}He was mixed with 2900 ml N_2 at 1 bar giving $m_0 = 1.8 \times 10^{-3}$ J T^{-1} m^{-3}. In the bag experiments, 80 ml ^{3}He was mixed with 920 ml N_2 at 1 bar giving $m_0 = 6.4 \times 10^{-3}$ J T^{-1} m^{-3} which is comparable to the m_0 of a 1 L sample of ^1H_2O at 1.5 T ($m_0 = 4.8 \times 10^{-3}$ J T^{-1} m^{-3}). In the cell experiments, 268 ml of ^{3}He at 1.2 atm pressure ($P = 38\%$) was used, giving a high $m_0 = 0.13$ J T^{-1} m^{-3}. The spherical cell was used in the quantitative analysis since its geometry is conducive to minimising the contribution from field inhomogeneity through good shimming. Moreover, the effects of dipolar demagnetising fields [4,5] can be neglected in this analysis as they average out to zero over a uniformly magnetised sphere.

A quadrature transmit–receive (T/R) low-pass birdcage coil was purposely built for these phantom studies; see Fig. 1a.

The birdcage had 7.5 cm inner radius, 11 cm shield radius and twelve 19-cm-long rungs. The rungs were split at their midpoints with 33 pF ceramic capacitors (Advanced Technical Ceramics, USA). The Q of the isolated coil disconnected from matching networks, (Q_0), was measured

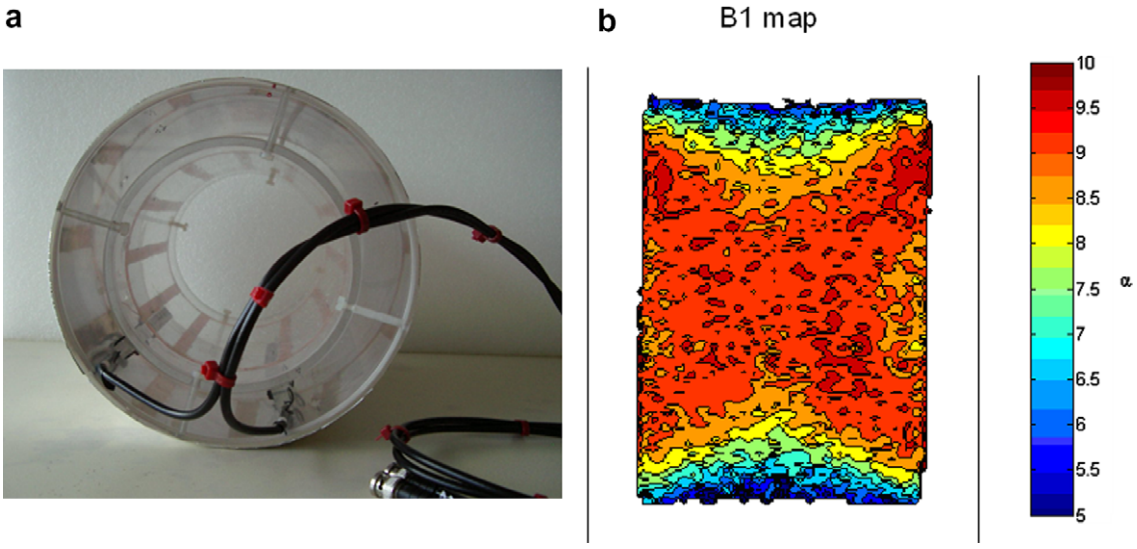

Fig. 1. (a) Picture of the quadrature low-pass T/R Birdcage Coil. (b) 2D flip angle homogeneity mapping to characterise the spatial flip angle in the coronal plane of a 3 L cylindrical flood phantom filled with 100 ml of HP ^{3}He and 2900 ml of N_2. The coil position is denoted by the lines.

on the bench with a network analyser (Agilent, 5601A) under weak coupling conditions. This was done by measurement of the S_{21} parameter whilst feeding a signal via a small pickup loop proximal to one end ring and picking up the signal at the other end ring with a second pick up loop. This unloaded Q was calculated as the ratio of the centre frequency to the 3 dB bandwidth of the resonance peak, resulting in $Q_0 = 500$.

The coil was then matched for a return loss better than 20 dB, and fed at orthogonal ports across two of the rung capacitors taking care to preserve the electrical symmetry of the coil using the symmetric driving arrangement described in Ref. [22]. The quality factor of the matched coil (Q_L) is the value that must be used in Eq. (1) to characterise the radiation-damping time constant, and was measured with the network analyser with the coil at magnet iso-centre resulting in $Q_L = 250$ at a frequency of 48.65 MHz (^{3}He resonant frequency). As expected from theory this value is approximately one-half that of the isolated coil.

Coupling between the two ports was also measured and found to be -26 dB, which is better than the -20 dB considered the minimum for adequate quadrature performance. The coil was operated in quadrature (circularly polarised) mode in all experiments. The input impedance of the preamp at 48.6 MHz is not necessarily 50 Ω, and it may be transformed in an unknown way by the transmission lines and hybrid splitter between the coil and the preamp. In such a case the actual Q_L of the whole circuit could differ from that measured at the coil ports. To this end, the input impedances of the circuit were measured by connecting the network analyser to the hybrid's 0° and 90° quadrature ports and were found to be, respectively, $57 + 20\mathrm{i}\ \Omega$ and $35 - 2\mathrm{i}\ \Omega$. The modest reflection occurring at these two ports has been accounted for by measuring the coil's Q_L while connected.

In order to estimate an upper limit on the filling factor, the ratio of the sample and coil volumes was calculated as $\eta_v = V_s/V_c$. This gives $\eta_v = 3.7\%$ for the glass cell and $\eta_v = 13.8\%$ for the bag. An estimate of η_E was then made from the ratio of RF magnetic energy of the sample and the total stored magnetic energy as detailed above, giving $\eta_E = 1.6\%$ for the glass cell and $\eta_E = 6.0\%$ for the bag.

The frequency shift test was also used to estimate η_{fs} by placing a 2 cm radius metal sphere in the coil (Eq. (11)). A shift in resonance of $f_\delta = 61$ kHz was recorded on the network analyser from a centre frequency of $f_0 = 48.64$ MHz which gives a value of $\eta_{fs} = 1.4\%$ for the glass cell and $\eta_{fs} = 5.0\%$ for the bag.

4. MR methods

4.1. B_1^+ mapping

A 2D B_1^+ mapping procedure was performed using spoiled gradient echo imaging sequences to characterise the coil homogeneity within the 3 L flood phantom. The sequence used had a short TR = 4 ms, 64 centric phase encode views, 10 mm slice thickness and a nominal flip angle of $\alpha \approx 9°$. The sequence should be fairly insensitive to radiation damping by virtue of the dephasing produced by the readout gradient and the short T_{acq} of 1.28 ms. Two images were acquired from the same slice in immediate succession. The T_1 relaxation between images can be neglected, however diffusion mixing of gas between the excited slice and the surroundings can present an additional source of error to the signal decay characteristics predicted by Eq. (3). This is especially the case with a sample in which diffusion is unrestricted as is the case here (measured $D = 0.9\ \mathrm{cm^2\ s^{-1}}$). This effect has been studied in detail previously in 2D imaging of ^{3}He and accurately quantified for phantoms of known diffusion coefficient by solving the Bloch–Torrey diffusion equation for the known slice excitation profile [23]. To account for the effect, a global estimate of α was taken from a non-slice selective implementation of the sequence. This nominal flip angle was then used to calculate and normalise for the effect on the signal decay of polarisation mixing by diffusion in/out of the slice, thus allowing the local α to be derived for each pixel from a two-point fit ($n = 1$ for image 1 and $n = 65$ for image 2) from Eq. (3).

4.2. Radiation-damping experiments

Radiation damping was probed by acquiring $n = 115$ sequential pulse-acquire data acquisitions with acquisition time T_{acq}. Each FID acquisition was followed by spoiling of the transverse magnetisation with a large crusher gradient (20 mT m^{-1} for 10 ms). The signal after the pre-amplifier was attenuated by 18 dB to avoid saturation of the receiver and possible clipping of the large transverse signal. Two sets of experiments were performed on the bag phantom and the cell in turn. Each set consisted of three individual experiments performed on the same phantom. The HP ^{3}He in the phantom was replenished between each experiment and the phantom repositioned in the same position such that the M_0 was approximately the same at the start of each. In each experiment the length of the transverse sampling period T_{acq} was varied: $T_{acq} = 4$, 256, 512 ms. The rationale is that longer acquisition times between excitation and spoiling provides a longer period for the transverse magnetisation to precess and set up a back reaction field and should thus demonstrate more radiation damping. The T_R between RF pulses was fixed at 741 ms in all experiments with a nominal flip angle of 7°. T_1 effects can be neglected due to the long sample T_1's and constant T_R used throughout. The received ^{3}He signal was then fitted to Eq. (3). This is an established means of calibrating α in HP gas NMR; for a constant α, the curve $\ln(M_n/M_0)$ should yield a linear slope of $\cos(\alpha)$.

A further experiment was performed on the spherical cell only, whereby the acquisition time was increased, to $T_{acq} = 2$ s. This was to provide further sensitivity to radiation damping and the longer T_{acq} also provides a finer spec-

tral resolution in the frequency domain in order to measure the line width as a function of magnetisation. In this experiment an estimate of the relative starting M_0 was made between acquisitions by measurement of the amplitude of the first time point of the nth FID from the previous acquisition. All data processing was performed off-line with Matlab code (Mathworks Inc., Natick, MA, USA).

5. Results

The birdcage coil has a highly homogeneous B_1^+ profile as demonstrated by the coronal slice flip angle map as shown in Fig. 1b.

Fig. 2 demonstrates the effect of varying T_{acq} with data from the bag phantom experiment shown for FID acquisition times of (a) 512 ms, (b) 256 ms and (c) 4 ms.

The plots show the log relation of Eq. (3) when plotted assuming no T_1 relaxation during T_R, hence the intercept through zero. The long T_{acq} curves deviate from linear behaviour in the early stage indicating a non-linear behaviour. Apparent flip angles, α, were fitted from the linear regions of each curve and were found to be 5.8°, 6.5° and 7.0°, respectively. This indicates that more magnetisation is returned to the longitudinal direction (more damping has occurred) when the transverse magnetisation is given a longer time to interact with the coil by means of a longer T_{acq}. These findings are consistent with those observed with samples of HP ^{3}He at $B_0 = 0.2$ T using a small pickup coil with high η and reasonable Q [9].

Fig. 3 shows the corresponding curves from the higher M_0 cell sample, the curves for all three T_{acq}'s show significant deviation from linear behaviour indicating a transient damping response as a function of the M_0. The $T_{acq} = 512$ ms data in particular shows very little decay between RF pulses indicating very little consumption of the longitudinal magnetisation and thus a severe occurrence of radiation damping. Fig. 4 shows the line shape of the FIDs acquired from the cell with $T_{acq} = 512$ ms with $n = 1$–135 pulses with transverse spoiling between pulses. As n increases, M_0 slowly decreases due to the non-recoverable spin population hence the extent of damping gradually diminishes, and this is manifested as an increasing relaxation time of the FID envelope. This is in agreement with experiments with water at 6.5 T [8]. For $n > 125$, noise becomes visible and the FID reaches a constant shape

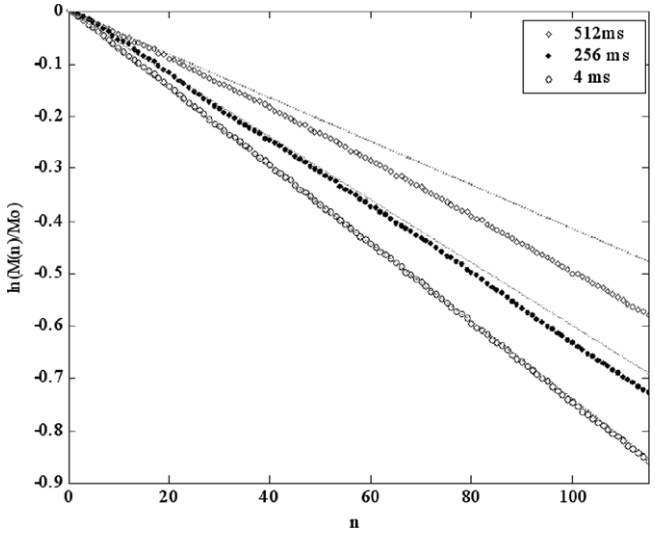

Fig. 2. Plots of $\ln(M(n)/M_0)$ for the FID acquisitions made with the bag phantom with T_{acq} times of (a) 512 ms, (b) 256 ms and a standard (c) 4 ms. Note the deviation of the long T_{acq} curves from a linear function (faint dotted lines) in the early stage and the different slopes of the curves in the later stage indicating differential, rate of magnetisation depletion due to radiation damping.

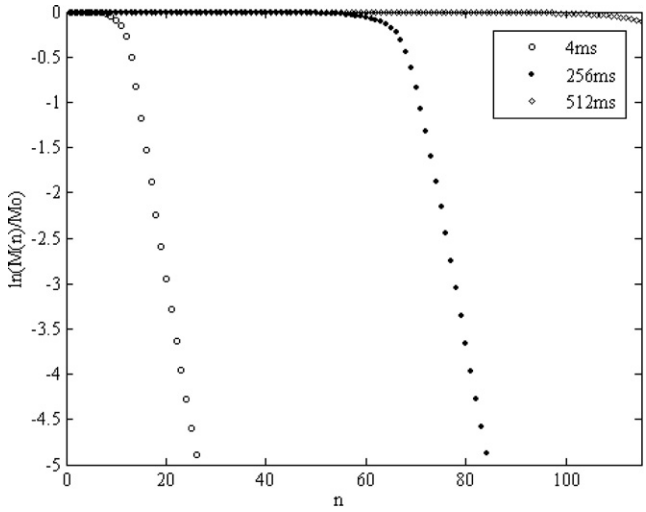

Fig. 3. Corresponding curves from the high M_0 spherical phantom sample. A much stronger effect is experienced even at low T_{acq} by virtue of the higher M_0 despite the lower geometrical contribution to the coil-sample filling factor of the smaller volume cell.

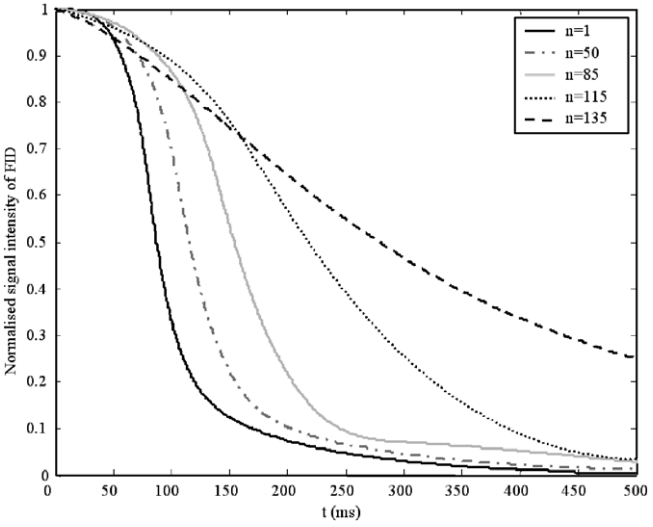

Fig. 4. Selected FIDs from the $T_{acq} = 512$ ms acquisition from the cell phantom. The FIDs become progressively less damped as M_0 decreases reaching a steady FID lineshape in the low polarisation limit ($n > 125$) where noise becomes visible.

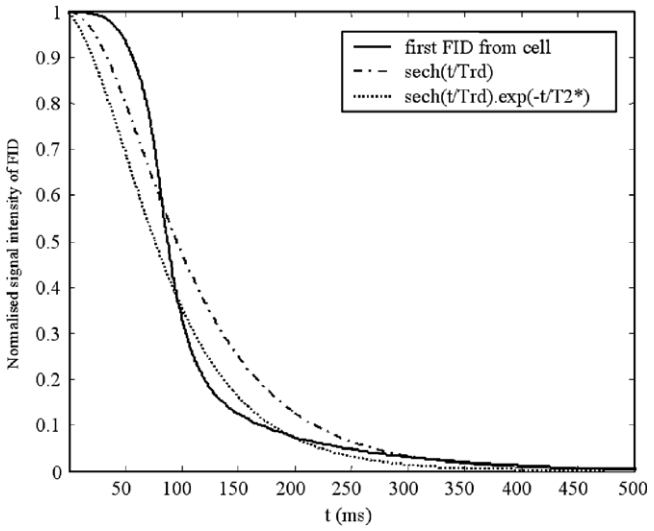

Fig. 5. Curve fitting of the first FID ($n = 1$) from the cell data set using a pure hyperbolic secant and a convolution of the same function with an exponential.

indicating radiation damping is negligible, allowing estimation of $T_2^* \approx 350$ ms which corresponds to a spectral peak of about 1 Hz assuming a Lorentzian line shape in the well shimmed spherical sample.

Fig. 5 shows attempts to fit the $n = 1$ FID to (i) $\mathrm{sech}(t/\tau_{rd})$ and (ii) $\mathrm{sech}(t/\tau_{rd}) * \exp(-t/T_2^*)$ using the notation of Gueron [8] with T_2^* estimated as 350 ms from the $n = 135$ FID. The FIDs are clearly not pure hyperbolic secants or exponential functions, and accurate determination of the damped relaxation will require solution of the coupled differential Bloch equations with an appropriate non-linear radiation damping term—see Section 6. The curve fit gives an estimate for $\eta_{RD} = 0.4\%$.

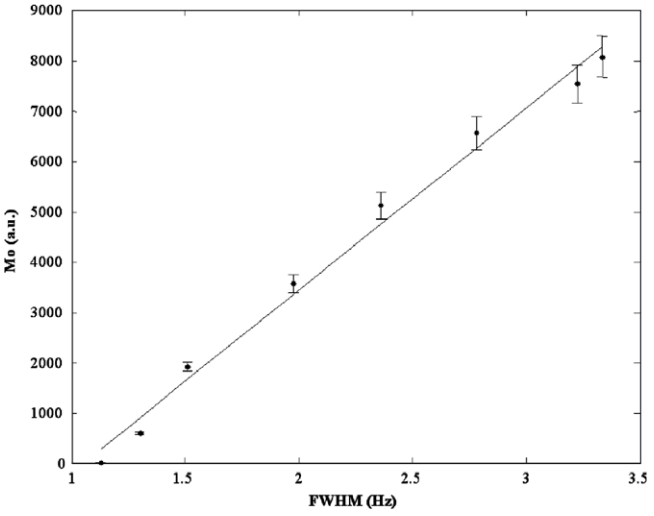

Fig. 6. Curve showing relative M_0 versus spectral FWHM of the 2 s long T_{acq} data from the cell. The straight line is a fit with a horizontal intercept equal to the low polarisation line width limit imposed by field inhomogeneity broadening.

The last set of experiments was performed using a series of $n = 1$–115 pulse-acquires with $T_{acq} = 2$ s to investigate the relationship between the line width and the magnetisation level. Fig. 6 depicts the plot of the relative M_0, as measured from the magnitude of the first sample point of each FID, versus the FWHM of the spectrum. The straight line is a linear fit to the data and the x intercept represents the FWHM (1.1 Hz) of the signal from the depolarised gas ($P < 1\%$), which is expected to be free from radiation damping. The data fits well with the reciprocal relation between τ_{rd} and M_0 of Eq. (1).

6. Discussion

In this work, radiation damping has been observed in a low-pass birdcage resonator with samples of hyperpolarised ^{3}He. It is believed that this is the first reported observation of the effect in a birdcage resonator with samples hyperpolarised or thermally polarised. In this work, it was assumed that radiation damping is the source of the non-linear behaviour in the FID. For the spherical sample with spatially uniform spin magnetisation it is safe to assume geometrical cancellation of the dipolar demagnetising field, which can produce unexpected spin echoes and FID distortion [2,4,5].

Coils with higher η such as single loop receivers and solenoids could be more sensitive to radiation damping at this field strength with HP gas samples and there is scope for in-vivo observation. The low η of the birdcage design (η estimated as <5% for a one litre sample inside this coil) could explain why radiation-damping effects have not been observed or at least reported before in thermally polarised birdcage experiments with other nuclei. As the γ of ^{1}H is 4/3 larger than that of ^{3}He, and the thermal M_0 of a standard 1 L water phantom is comparable to that used in the HP ^{3}He bag phantom experiments which displayed-damping effects Fig. 2, then it might be expected that these effects are present in H_2O NMR at this field strength. One factor that may inhibit the observation of radiation damping in ^{1}H MR with birdcage resonators are sample losses, which reduce the loaded coil Q_L. These losses are non-existent with our high-Q resonator and gas phantom. This theory will be investigated in further work with ^{1}H birdcage coils using ^{1}H samples with minimal dielectric losses (e.g. C_6H_{12}). Another factor that favours radiation damping in the ^{3}He experiments is the long T_2^* (≈350 ms) in the small spherical cell which allows transverse coherence to be preserved and facilitates long back reaction times for the associated radiation-damping field. In a 1 L sample of ^{1}H solution such a long T_2^* would require a very good shim but should be attainable with a spherical sample. It will also be of interest to investigate radiation-damping effects in birdcage coils with HP ^{3}He at higher B_0 where T_2^* is smaller; experiments with a high-pass birdcage at 3 T are planned. It is anticipated that in vivo radiation-damping effects in birdcage coils will be weaker by virtue of the low T_2^* (20–30 ms) found with ^{3}He in the lungs at 1.5 T [24]. Nevertheless an awareness of the presence of radiation

damping is advised in HP gas MRI as it could have major implications in RF calibration experiments as demonstrated here, since accurate knowledge of the flip angle is imperative. If radiation damping is found to cause persistent problems suppression schemes can be sought, such as active electronic feedback mechanisms to reduce the Q [25].

Exact solution of the non-linear Bloch equations and calculation of the damping time constant was not the objective of this work. Nevertheless the reciprocal relation between the FWHM and the M_0 as demonstrated by Fig. 6 indicates the original model presented by Bloembergen and Pound [3] in Eq. (1) serves as a reasonable approximation when used with the appropriate SI units [8]. The curve fits of Fig. 5 show that the FID is not a true hyperbolic secant, however, if the initial slowly decaying response of the FID were to be ignored, then the steeply sloping region of the solid curve in Fig. 5 does resemble a hyperbolic secant function with a shorter time constant than those fitted by considering the whole of the FID. A full solution (numerical or analytical) to the non-linear Bloch equations for this experimental set up would require deconvolution of T_2^* line broadening from radiation damping. This could be pursued in further work with appropriate models of the field inhomogeneity broadening other than the simple Lorentzian assumed here. This serves as a good starting point assuming motion narrowing by diffusion of ^{3}He in the spherical cell and a good shim as indicated by the 1 Hz line width of the weakly polarised signal. However the simple curve fits of Fig. 5 yield an estimate of $\eta = 0.4\%$ which is a factor of four smaller than the estimate from EM theory, 1.6%, and that from the frequency shift method, (1.4%). This discrepancy may be due to an inaccurate basis for the lineshape as described above, or the fact that existing descriptions of radiation damping assume linearly polarised fields, while resonators that support circular polarization are doubly effective at receiving, as well as emitting, with circular polarization. This suggests a revision of Eq. (1) with the constant 2 moved to the numerator, i.e., $\tau_{rd} = 2 \cdot (\pi\gamma\eta M_0 Q)^{-1}$. All measured values are within the theoretical upper limit given by the ratio of cell volume to total coil volume (shield included), which is equal to 3.7%.

The exact solution may provide an accurate means of characterising the birdcage filling factor which is still a rather grey area as highlighted by Tropp [13] and the index of efficiency may prove to be a better comparable factor. Provided the coil Q and sample magnetisation can be accurately measured then fitting of the damping time constant in this way may provide some additional experimental validation of the different theories proposed [12,13].

Acknowledgment

GE Healthcare for support with polarization apparatus. Spectra Gases for support with ^{3}He gas. Funding: EPSRC, UK. Grant # GR/S81834/01(P) and # EP/D070252/1.

References

[1] F. Bloch, Nuclear induction, Physical Review 70 (1946) 460.
[2] G. Deville, M. Bernier, J.M. Delrieux, NMR multiple echoes observed in solid ^{3}He, Physical Review B 19 (1979) 5666.
[3] N. Bloembergen, R.V. Pound, Radiation damping in magnetic resonance experiments, Physical Review 95 (1954) 8.
[4] Q. He, W. Richter, S. Vathyam, W.S. Warren, Intermolecular multiple-quantum coherences and cross correlations in solution nuclear magnetic resonance, The Journal of Chemical Physics 98 (1993) 6779.
[5] M.A. McCoy, W.S. Warren, Three-quantum nuclear magnetic resonance spectroscopy of liquid water: intermolecular multiple-quantum coherence generated by spin–cavity coupling, The Journal of Chemical Physics 93 (1990) 858.
[6] V.V. Krishnan, Radiation damping in microcoil NMR probes, Journal of Magnetic Resonance 179 (2006) 294.
[7] D.I. Hoult, N.S. Ginsberg, The quantum origins of the free induction decay signal and spin noise, Journal of Magnetic Resonance 148 (2001) 182.
[8] M. Gueron, J.L. Leroy, NMR of water protons. The detection of their nuclear-spin noise, and a simple determination of absolute probe sensitivity based on radiation damping, Journal of Magnetic Resonance 85 (1989) 209.
[9] G.P. Wong, C.H. Tseng, V.R. Pomeroy, R.W. Mair, D.P. Hinton, D. Hoffmann, R.E. Stoner, F.W. Hersman, D.G. Cory, R.L. Walsworth, A system for low field imaging of laser-polarized noble gas, Journal of Magnetic Resonance 141 (1999) 217.
[10] A. Oregioni, T.R. Eykyn, N. Hosny, G.S. Payne, M.O. Leach, Adiabatic half-passage pulses for measuring the polarization of highly non-equilibrium spin-systems, Chemical Physics Letters 414 (2005) 102.
[11] C.E. Hayes, W.A. Edelstein, J.F. Schenck, O.M. Mueller, M. Eash, An efficient, highly homogeneous radiofrequency coil for whole-body NMR imaging at 1.5 T, Journal of Magnetic Resonance 63 (1985) 622–628.
[12] F.D. Doty, J. George Entzminger, C.D. Hauck, J.P. Staab, Practical aspects of birdcage coils, Journal of Magnetic Resonance 138 (1999) 144–154.
[13] J.S. Tropp, Radiation Damping and Reciprocity in Magnetic Resonance Reception, in: Proceedings of the 12th Scientific Meeting 2004, International Society for Magnetic Resonance in Medicine, Kyoto, p. 1646.
[14] S. Bloom, Effects of radiation damping on spin dynamics, Journal of Applied Physics 28 (1957) 800.
[15] A.G. Sobol, G. Wider, H. Iwai, K. Wuthrich, Solvent magnetization artifacts in high-field NMR studies of macromolecular hydration, Journal of Magnetic Resonance 130 (1998) 262.
[16] M.P. Augustine, Transient properties of radiation damping, Progress in Nuclear Magnetic Resonance Spectroscopy 40 (2002) 111.
[17] D.I. Hoult, The principle of reciprocity in signal strength calculations—A mathematical guide, Concepts in Magnetic Resonance 12 (2000) 173–187.
[18] T.R. Gentile, D.R. Rich, A.K. Thompson, W.M. Snow, G.L. Jones, Compressing spin-polarized ^{3}He with a modified diaphragm pump, Journal of Research of the National Institute of Standards and Technology 106 (2001) 709–729.
[19] A. Abragam, The Principles of Nuclear Magnetism, Clarendon Press, Oxford, 1961.
[20] N. De Zanche, P.S. Allen, Sensitivity calculations and comparisons for shielded elliptical and circular birdcage coils, Magnetic Resonance in Medicine 47 (2002) 364–371.
[21] J. Tropp, Dissipation, resistance, and rational impedance matching for TEM and birdcage resonators, Concepts in Magnetic Resonance 15 (2002) 177–188.
[22] P.B. Roemer, W.A. Edelstein, C.E. Hayes, M.G. Eash, Method for providing multiple coaxial cable connections to a radio-frequency antenna without baluns, US patent 4887039, 1989.

[23] J.M. Wild, N. Woodhouse, M.N.J. Paley, S. Fichele, Z. Said, L. Kasuboski, E.J.R. van Beek, Comparison between 2D and 3D gradient-echo sequences for MRI of human lung ventilation with hyperpolarized ^{3}He, Magnetic Resonance in Medicine 52 (2004) 673–678.

[24] J.M. Wild, S. Fichele, N. Woodhouse, M.N.J. Paley, P.D. Griffiths, A. Swift, E.J.R. van Beek, Assessment and compensation of macroscopic field inhomogeneity artifacts in gradient echo ^{3}He MRI, in: Proceedings of Helion02, International Workshop, Oppenheim, Germany, 2002.

[25] A. Louis-Joseph, D. Abergel, J.-Y. Lallemand, Neutralization of radiation damping by selective feedback on a 400 MHz NMR spectrometer, Journal of Biomolecular NMR 5 (1995) 212.